Nanoshocks in Molecular Materials

DANA D. DLOTT*

School of Chemical Sciences, University of Illinois at Urbana-Champaign, Box 01-6 CLSL, 600 South Goodwin Avenue, Urbana, Illinois 61801

ABSTRACT

Nanoshocks are tiny but powerful laser-driven shock waves that can be used to produce large-amplitude compression in molecular materials on the picosecond time scale. When coupled with ultrafast molecular spectroscopy, the molecular response to nanoshocks can be probed in detail. Simple molecular systems (anthracene crystals) are used to characterize the nanoshock pulses. Well-characterized nanoshocks are used to study complex phenomena such as shock-induced chemical reactions, shock-induced orientation of energetic solids, and shock compression of organic polymers and proteins.

Introduction

Optical pump—probe techniques are widely used to study molecular dynamics in condensed phases. In the shock wave spectroscopy technique developed by my research group at the University of Illinois,[1] the "pump" pulse is not an optical pulse, but rather a short-duration shock pulse which produces ultrafast large-amplitude compression of the sample. The shocked material is about 1 ng, and the shock duration is about 1 ns—hence the name "nanoshock".

Shock compression has been used for the scientific study of condensed matter since about 1955.[2] A typical shock wave experiment is a single-shot event, where the shock is generated by a gun, a bomb, or a huge laser facility. These shock events can be studied using single-shot spectroscopic techniques, and a recent review of progress in this field has been published.[3] Our intention in developing the nanoshock technique was to make shock wave spectroscopy more like conventional ultrafast spectroscopy, where a tabletop laser is used to obtain dynamical spectra at high repetition rates. A convenient shock spectroscopy technique will have many fundamental and practical applications in chemical and biological sciences.

What Is a Shock Wave?

Shock waves are produced in condensed matter impacted by projectiles traveling, at minimum, a reasonable fraction of the speed of sound.[2,4] A shock front traverses the sample at supersonic velocity, where the density ρ_s behind the front is greater than the ambient density ρ_0. In explosive-generated or laser-generated shocks, the "projectile" is the recoil from rapid expansion of the exploding material. Shock compression is an irreversible adiabatic process. For a wide variety of materials, the relationship between the projectile velocity U_p and the shock velocity U_s has been measured and tabulated.[5] This relationship is termed the Hugoniot, or shock adiabat. From elementary considerations of conservation of mass, momentum, and energy, the Hugoniot—Rankine relations can be derived,[5] which relate the density ρ_s, pressure P_s, and energy E_s of the shocked material to the values ρ_0, P_0, and E_0 of unshocked material. A more complicated problem is the temperature of a shocked material, which depends on the path taken to the compressed final state and on the lattice anharmonicity. The Grüneisen parameter is a convenient measure of the degree of anharmonicity, which can be determined from thermodynamic or acoustic measurements.[4]

Consider the case of anthracene, worked out in detail in ref 6, which is representative of many (nonporous) chemical solids. The speed of sound is 3.5 km/s.[5,7] In other useful units, the speed is 3.5 mm/μs or 3.5 nm/ps. For impact by a projectile traveling at one-tenth sonic speed (0.35 km/s; about Mach 1), Hugoniot data[5,7] show that material behind the shock front is compressed to a density ~1.1 times greater than normal. The shock velocity will be about 1.1 times the sonic velocity, or about 3.9 km/s (3.9 nm/ps). The shock pressure will be about 1.7 GPa (17 000 atm, or 17 kbar). The shock temperature rise will be about 140 °C for a sample initially at ambient temperature.[6]

Like the ideal gas law, the Hugoniot—Rankine equations tell us nothing about the behavior of the shocked molecules themselves, so analytical models such as those developed by our group[8-10] and others,[11-13] or molecular dynamics simulations[14-17] are used. Most simulations, which model the propagation of ideal shock fronts over nanometer distances, show the width of shock fronts to be just a few molecular diameters. Such sharp shock fronts would preferentially excite phonons and lower energy molecular vibrations, producing highly nonequilibrium vibrational populations.[8,9,18] Just recently, experiments have seen shock front rise times considerably less than 1 ns.[18,19] However, there is a sizable literature on the impact of large projectiles on metal and other materials which show shock fronts with complicated waveforms rising on the 10 ns to 1 μs time scales.[2,20] It is clear that more work is needed to reconcile these microscopic and macroscopic pictures.

Why Use Shock Waves?

Interesting chemical events such as chemical bond formation or bond breaking, macromolecule conformational dynamics, and so forth almost always involve large-

---

Dana D. Dlott was born in Los Angeles in 1952. He received his undergraduate degree from Columbia University and his Ph.D. with Prof. M. D. Fayer at Stanford University. In 1979, he joined the faculty of the University of Illinois at Urbana-Champaign. His other research interests include vibrational energy transfer in condensed phases, protein dynamics, and laser interactions with photothermal imaging materials.

* Tel.: 217-333-3574. Fax: 217-244-3186. E-mail: dlott@scs.uiuc.edu.

amplitude motion (typically angstroms) in the higher energy regions of the potential energy surface. Light pulses used in ultrafast spectroscopy do not directly produce large-amplitude motion. However, there are a few tricks which let researchers make large-amplitude motions with light, almost all involving electronic excitation. In photochemistry, light absorption produces a dissociative electronic state. In polar solvation,[21] the excited electronic state has a large dipole moment, which triggers large-amplitude motions in the surrounding solvent. In our experiments, we use light pulses to trigger an explosion to ablate a thin layer which generates a shock wave, directly producing large-amplitude displacements, and instantaneously driving the system high up the potential energy surface. Quite high temperatures can be generated as well. Shock pulses may also be used to initiate a fast cycle of ultrafast heating and ultrafast cooling, which can quench amorphous materials into metastable states. The attainable displacements and temperatures are not trivial. Nanoshock compression of 20% and temperature jumps of hundreds of degrees may be attained in a few tens of picoseconds. Nanoshock unloading produces cooling rates of several hundred billion degrees per second. The distance between two anthracene molecules in a crystal (∼10 Å) can be reduced by ∼2 Å in a few picoseconds; a 40-Å-diameter protein such as myoglobin (Mb) can be compressed by ∼8 Å.[3] Simulating the dynamics of electronically excited molecules is a tremendously complicated problem unless the excitations are treated in a completely ad hoc manner, as in classical simulations. A fast uniaxial compression is easily treated in a molecular simulation.

Nanoshock Technique

Simply focus an intense laser pulse on a solid and—bam!— there is an explosion which produces a shock wave. But much more is needed to have a precision tool for chemical research. A well-characterized shock is desired, with a steeply rising planar shock front running at a constant velocity.[1] Powerful spectroscopic techniques capable of probing the thin region near the shock front ordinarily involve extensive signal averaging, so reproducible shock pulses should be generated at a high repetition rate. Shock target assembly methods should allow the study of interesting chemical systems.

The time resolution problem[18,22,23] is worthy of further discussion. Consider Figure 1, a cross section of one element of a target array, where a shock is launched from left to right. The sample, also termed an optical nanogauge, is a thin layer inside an impedance-matched[5] sandwich. Dynamical processes occurring in the sample layer can be distinguished from the other layers by the sample's characteristic spectroscopic signature, e.g., by using vibrational spectroscopy or by doping the sample with a dye. At the present time, the thinnest samples we use are about 400 nm thick. The shock transits such samples in about 100 ps. Optical probe pulses, by contrast, would transit the same sample in about 2 fs, as if the shock
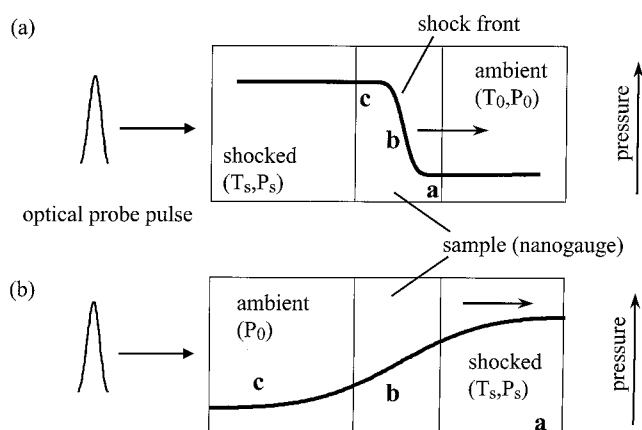
FIGURE 1. A shock front moving through a sandwich containing a thin sample layer, the optical nanogauge. The shock jumps the sample from ambient temperature and pressure T_0, P_0 to T_s, P_s. (a) A shock front b with a fast rise (relative to the transit time) cuts the sample (shaded region) into two parts, a and c. (b) The nanoshock pulse falls more slowly than it rises. The pressure declines slowly and uniformly throughout the nanogauge layer.
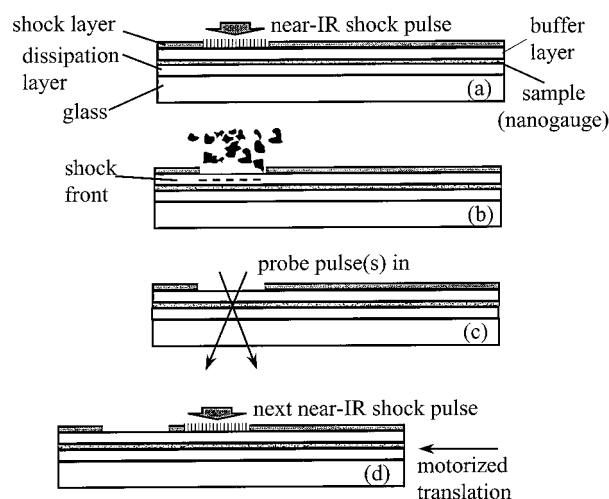
FIGURE 2. A near-IR pulse ablates the shock layer, consisting of a near-IR dye and a decomposable polymer, launching a shock through the buffer layer, the sample layer, and the dissipation layer. After the shock layer has ablated away, time-delayed pulses probe the sample layer. After a spectrum is obtained, the array is translated to a fresh spot.

front were standing still. At the instant the shock front reaches the end of the sample layer, an optical probe pulse would see some molecules which were shocked 100 ps earlier and some molecules which were just then shocked. Spectra obtained by the probe pulses would represent an average over an ∼100-ps time window. In contrast to ordinary laser experiments, where the time resolution is determined mainly by optical pulse durations, this severe transit time mismatch means the time resolution of shock experiments is determined mainly by the shock transit time through the sample.

Figure 2 is a schematic of a typical shock target array used in our experiments,[22] consisting of a glass substrate 10 × 10 cm², coated with a thin sample layer (Figure 2a). Sometimes a dissipation layer is placed between the sample and the glass to eliminate shock reflections from
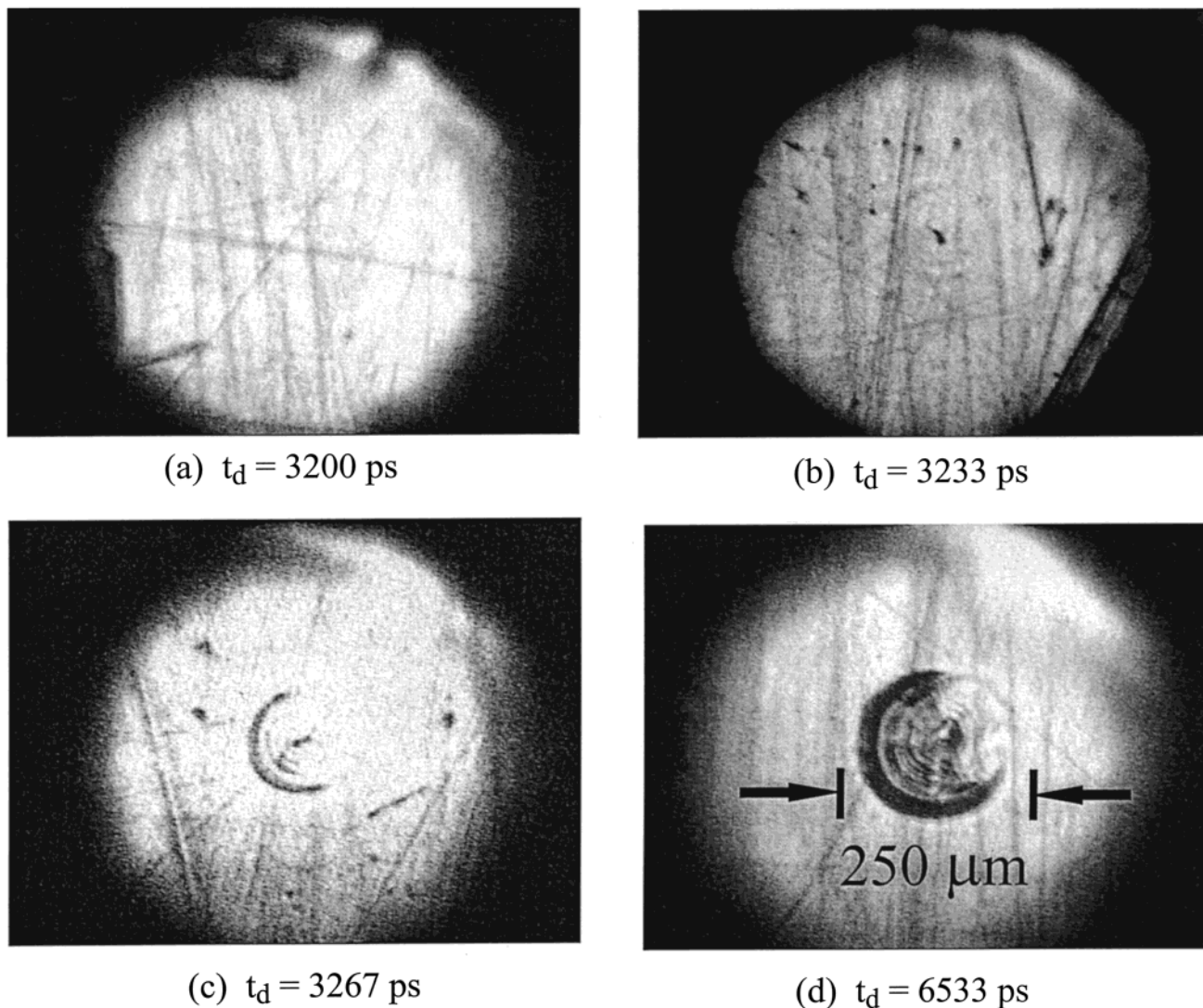
(a) $t_d = 3200$ ps

(b) $t_d = 3233$ ps

(c) $t_d = 3267$ ps

250 μm

(d) $t_d = 6533$ ps

FIGURE 3. Time-resolved microscope images of a 200-μm-diameter nanoshock emerging from an opaque aluminum layer into a transparent polymer layer. (a) At $t = 3200$ ps, the shock front is inside the aluminum. (b and c) In the next few tens of picoseconds, the front emerges, driving a cylindrical aluminum ram into the polymer. (d) After several nanoseconds the ram has been driven a few micrometers into the polymer.

the glass. A buffer layer and a shock generation layer are coated on top of the sample. The shock generation layer consists of a decomposable polymer binder doped with a near-infrared (near-IR) dye, which absorbs ∼1-μm light from a solid-state laser such as Nd:YLF (YLF denotes yttrium lithium fluoride) or 0.8-μm light from a Ti:sapphire laser. A near-IR shock generation pulse ablates a small spot in the shock layer (Figure 2a). Ablation recoil drives a shock wave through the buffer layer into the sample (Figure 2b). During the first 10 μm of propagation, the shock front is approximately planar. The initial shock front has a somewhat slower rise time, which depends on the laser pulse duration and the shock layer thickness and absorption coefficient. The higher pressure trailing edge moves faster than the lower pressure leading edge, so the shock front steepens as it is driven through the 7-μm-thick buffer layer.[22,24,25] The buffer layer delays the shock arrival at the sample by a few nanoseconds (Figure 2b), time enough for ablation debris to dissipate.[22] When the debris clears, time-delayed probe pulses monitor shock dynamics

of the sample (Figure 2c). A new target element is moved into position by a motorized driver (Figure 2d). The shock and probe process is repeated at a repetition rate of about 100 shocks per second. A single target array consists of about one million individual shock elements, each about 200 μm in diameter. Shock pressures in the range of 0−5 GPa with durations of 0.5−4 ns have been generated.[6,22] Using more powerful lasers, opaque metal shock layers, and confined geometries, pressures up to 12 GPa and durations of tens of nanoseconds have been attained.[26]

Figure 3 shows some images of a nanoshock obtained with an ultrafast microscope, which is simply a microscope illuminated by a 30-ps white light pulse.[26] In this experiment, we are looking through a transparent polymer layer onto the surface of an opaque aluminum shock generation layer. As the shock emerges from the metal, a tiny metal cylinder (a "ram") 200 μm in diameter is driven into the transparent sample. It is like hitting the sample with a hammer moving in the 0−1 km/s range.
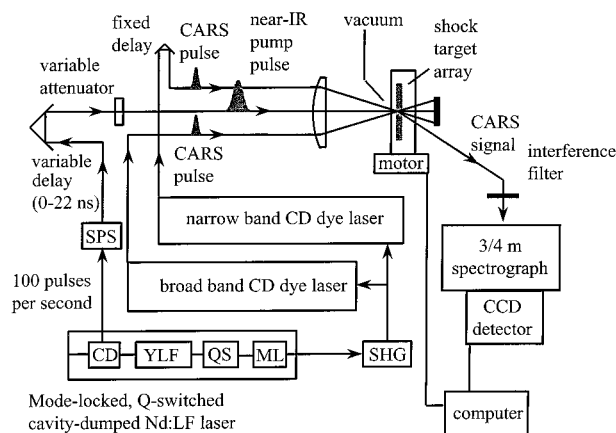
FIGURE 4. Block diagram of the nanoshock laser system. Near-IR pump pulses repetitively produce shocks as the target array is scanned. Simultaneous narrowband and broadband dye laser pulses generate CARS spectra. CD = electrooptic cavity dumper; YLF = Nd:YLF laser head; QS = Q-switch; ML = mode locker; SPS = single pulse selector; SHG = second harmonic generating crystal; CCD = charge-coupled array detector.

The nanoshock laser apparatus[22] is diagrammed in Figure 4. A solid-state laser (Nd:YLF) produces 80-ps near-IR shock generation pulses. The shock pulse energy is 0.1–0.5 mJ, a pulse energy which is readily obtained from available tabletop ultrafast lasers. Some of the Nd:YLF laser output is frequency doubled to generate probe pulses of a few microjoules energy from a pair of dye lasers. A variety of spectroscopic probing techniques can be realized with two independently tunable dye lasers. To obtain vibrational spectra, broadband multiplex coherent Raman scattering[27] (CARS) is used, where one dye laser, with a narrow bandwidth, is tuned to frequency ω_L and the second, with a broad bandwidth ω_{BB}, is tuned so that several molecular vibrational transitions lie in the frequency range $\omega_L - \omega_{BB}$. Coherent techniques such as CARS provide high-quality spectra despite the thin sample layer and the nearby exploding shock layer. Some typical CARS spectra are shown in Figure 5 for a 700-nm-thick sample of anthracene. These spectra are obtained by averaging ~5000 laser shots over a 1-min time interval. Several vibrational transitions in the 1100–1600-cm^{-1} range are observed.[1] When shocked, these transitions frequency-shift and broaden. The most intense transition, ν_4 at ~1404 cm^{-1}, has been studied by us in static high-pressure and high-temperature cells.[22] The frequency shift is usually an explicit function of density rather than pressure, so the shift expected in a shock experiment can be inferred from static experiments at the same density.[6] An expanded view of ν_4 is shown in Figure 5b. To a reasonable degree of accuracy (~10%), the frequency shift can be used to determine the pressure and the spectral width to determine the temperature.[6,22] Here the shift is ~16 cm^{-1}, and the transition roughly doubles in width. The spectrum in Figure 5 gives the pressure as ~4.2 GPa and the temperature as ~350 °C.
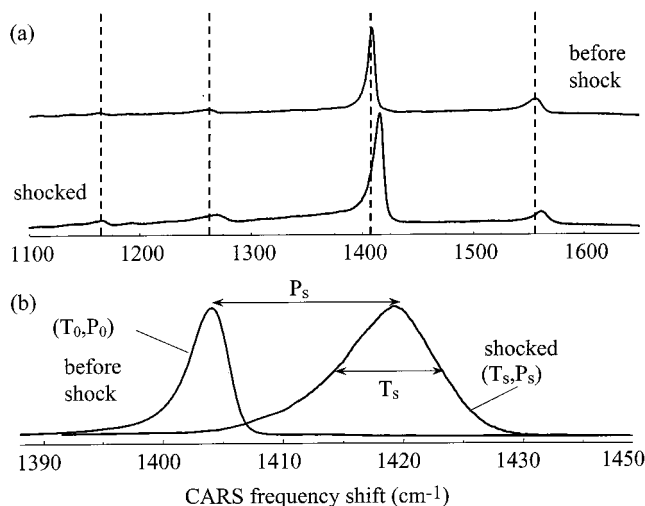

FIGURE 5. (a) Coherent anti-Stokes Raman (CARS) spectrum of a 700-nm layer of polycrystalline anthracene in a shock target array. The "shocked" spectrum is obtained 200 ps after the shock enters the anthracene. Each spectrum is the average of ~5000 laser shots. (b) Expanded view of the intense ν_4 transition near 1404 cm^{-1}. The frequency shift can be used to estimate pressure P_s. The width can be used to estimate temperature T_s. Here, $P_s \approx 4.2$ GPa and $T_s \approx 350$ °C.
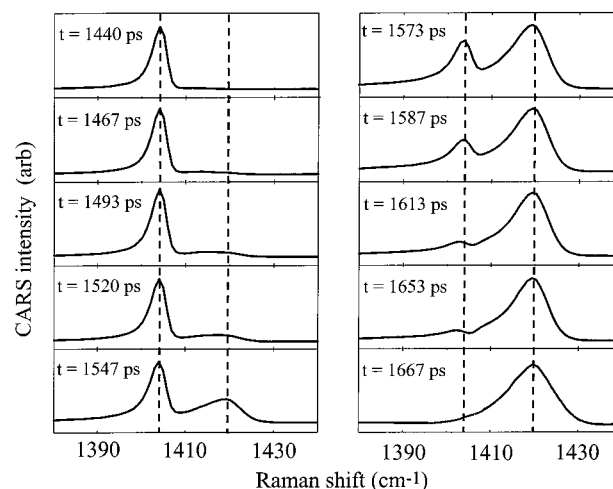

FIGURE 6. A time series of CARS spectra of the ν_4 transition of a 700-nm anthracene layer with a 4.2-GPa shock. The shock enters the anthracene layer at $t \approx 1.45$ ns, transits for 180 ps, and exits at $t \approx 1.63$ ns. Two distinct spectral transitions are observed when the shock front is within the sample, corresponding to ambient and shocked anthracene. The shock front neatly divides the layer into two parts, as in Figure 1a. A detailed analysis performed by Tas et al.[18] indicates that the shock front rise time is <25 ps.

Shock Rise Time and Fall Time

Anthracene was used to measure the shock front rise time and to optimize shock and buffer layers to minimize the rise time. Some representative data from our current design[23] are shown in Figure 6. The shock front arrives at the anthracene layer at about 1.45 ns, transits for 180 ps, and exits at about 1.63 ns. Times are always given relative to the arrival of the near-IR pulse which generates the shock. The remarkable feature in Figure 6 is that the Raman transition appears as two distinct peaks when the shock front is inside the sample layer. The two peaks
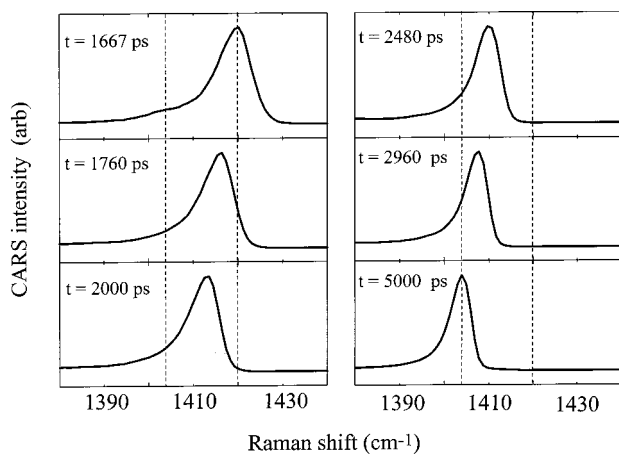
FIGURE 7. A time-series of CARS spectra of the ν_4 transition of a 700-nm anthracene layer during nanoshock unloading from 4.2 GPa. The first spectrum is the same as the last spectrum in Figure 6. The red-shifting indicates pressure release, and the narrowing indicates cooling by adiabatic expansion at a rate of a few hundred billion degrees per second.
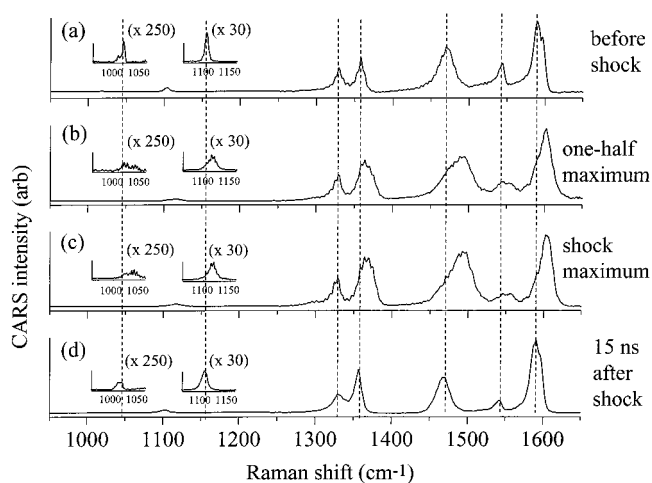

FIGURE 8. CARS spectra of nanoshocked NTO, an insensitive energetic material. As the nanoshock unloads, peak intensities and widths begin to permanently change on the ~10-ns time scale, indicating shock-induced orientation of the polycrystals in the sample layer.

correspond to ambient and shocked anthracene. As the shock front progresses through the sample layer, the intensity of the ambient peak declines and the intensity of the shocked peak increases. These data show that the shock front neatly divides the sample layer into two parts, as depicted in Figure 1a. Therefore, the shock front rise time is quite a bit less than the 180-ps transit time. This shock compression process is strongly irreversible, since the driving pressure is much greater than the internal sample pressure. A detailed numerical analysis[23] of the data in Figure 6 showed that the shock front was <25 ps wide. An anthracene molecule is about 1 nm, so the shock front width in this case is less than 25 anthracene molecules.[18,23]

Figure 7 shows CARS spectra during the nanoshock unloading process.[23] Unloading is a reversible process,[4] and nanoshock decay is always more gradual than the rise of the compression shock front.[4] As shown in Figure 1b, the pressure during unloading is almost the same everywhere in the sample layer. At every time, only a single Raman transition is observed, which red-shifts and narrows over a time period of a few nanoseconds.[23] The red-shifting indicates pressure release, and the narrowing indicates cooling. In Figure 7, the pressure decreases from 4.2 GPa back to 1 atm, and the temperature decreases from 350 to about 75 °C. Just as in the more familiar process of adiabatic expansion of a gas, solid-state expansion produces rapid cooling. This cooling, from about 350 back to 25 °C, occurs at a fantastic rate of a few hundred billion degrees per second, which is believed to be the fastest cooling process ever observed.

Nanoshock Pulses

The anthracene results show that ultrafast shock pulses can be reproducibly and repetitively repetitively generated at high repetition rates with a moderate power ultrafast laser. In considering research applications for nanoshocks,

there are three ways to think about the nanoshock technique:[1] (1) *A sudden ultrafast uniaxial compression.* The rise time is presently known to be <25 ps, but it might be much faster. (2) *A sudden jump to high pressure and high temperature.* An equilibrium value of *P* is established after the uniaxial compression relaxes to a hydrostatic compression. An equilibrium value of *T* is established after the nonequilibrium vibrational population (the shock preferentially excites phonons and lower frequency molecular vibrations) relaxes to a thermal distribution.[8,9,18] (3) *A fast cycle of heating and cooling (quenching).*

Nanoshock spectroscopy of condensed matter molecular dynamics may be viewed as an alternative to the more usual studies of photochemistry or other electronic excited-state processes. With nanoshocks, the emphasis is on fast mechanical and thermochemical processes occurring in the electronic ground state.

Energetic Materials

A natural application for shock spectroscopy is understanding shock initiation of high explosives. Two examples are provided from current research.

The insensitive energetic material 3-nitro-1,2,4-triazol-5-one (NTO) is a recently developed explosive which is both powerful and relatively safe to handle.[28] A randomly oriented polycrystalline thin film of NTO, 1 μm thick, was deposited on a shock target array by spraying from an acetone solution.[29] The ~5 GPa nanoshocks were too weak to initiate explosive reactions in the NTO. Figure 8 shows a series of CARS spectra. During the maximum of the nanoshock pulse, NTO transitions frequency shift, some to the red and some to the blue.[29] A blue shift is normal, but red-shifting is sometimes seen for vibrations involving hydrogen-bonded functional groups. The most interesting features of Figure 8 are the permanent changes in Raman intensities after the shock. For example, compare the intensity ratio of the two peaks in the 1300−1400-cm^{-1} range in Figure 8a and 8d. The Raman intensity changes
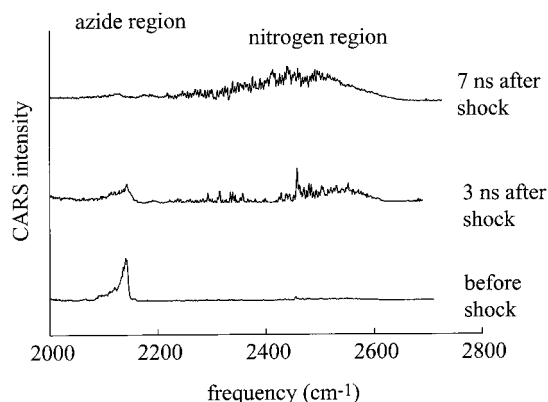
FIGURE 9. N—N bond cleavage induced by ~5-GPa nanoshocks in a 1-μm-thick layer of C_3N_{12}. The azide symmetric stretching transition is seen at ~2160 cm^{-1}. In the nanoseconds after shock, the azide transition loses intensity, and a broad transition in the 2300—2500-cm^{-1} range, associated with condensed phase N_2 in a broad inhomogeneous distribution of environments, is observed.

occur over a period of ~10 ns, beginning just as the nanoshock starts to unload.[29] Comparing these spectra to oriented single crystals showed that nanoshock unloading was partially orienting the nanocrystals in the NTO layer, faster than the time scale for initiating chemical reactions. Since the sensitivity of explosive crystals to shock initiation may depend dramatically on the orientation of the crystal relative to the direction of shock propagation,[30] fast shock-induced orientation may substantially increase or decrease the sensitivity to shock initiation.[29]

It is difficult to explode energetic materials with short duration nanoshocks. The likelihood of initiating an explosive is usually proportional to $P^p\tau$, where τ is the shock duration,[31] so nanoshock initiation requires higher pressures than the usual explosive initiator, which is ordinarily a microsecond duration shock. As an alternative, very sensitive explosives must be studied. We chose a very sensitive azide (C_3N_{12}), from the family $M_x(N_3)_y$, which presumably decomposes initially by nitrile-producing reactions such as $C_3(N_3)_4 \rightarrow C_3(N_3)_3-N + N_2$, and ultimately to carbon soot, N_2, and C—N polymers.[32] C_3N_{12} was selected for ease of fabricating thin layers. The azide symmetric stretching transition in Figure 9 is seen at ~2160 cm^{-1}. A few nanoseconds after the 5-GPa shock, the azide transition has broadened and decreased in amplitude, and a broad feature has grown in the 2300—2500-cm^{-1} range. The center frequency of this broad feature is similar to frequencies for N_2 in condensed phases (e.g., liquid N_2 at 2326 cm^{-1}). The spectral width is attributed to inhomogeneous broadening, expected to be severe since the crystalline lattice is destroyed by the fast decomposition reaction.[33]

Ultrafast Mechanical Relaxation in Polymers and Proteins

A microscopic understanding of fast large-amplitude structural dynamics of amorphous materials helps extend current work beyond the linear response regime and might be relevant to practical problems such as impact
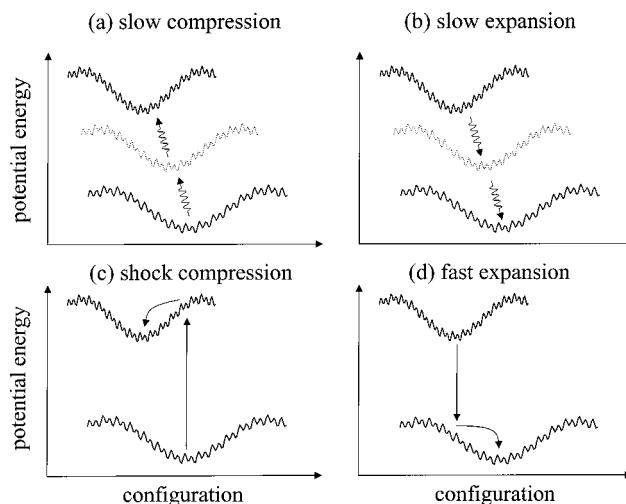

FIGURE 10. Potential energy landscapes for compression of an amorphous solid. (a, b) Slow compression or expansion is a gradual evolution along a series of different landscapes. The global minimum of compressed landscapes is displaced from the ambient landscapes along the configuration coordinate. (c) Fast shock compression is a vertical transition from the ambient to a compressed landscape, followed by dynamical structural evolution on the compressed landscape. (d) Fast expansion is a vertical transition to the ambient landscape, followed by structural evolution on the ambient landscape.

resistance of polymers and, in the medical realm, wound trauma induced by projectiles or the effects on biological tissues of shock waves generated in pulsed laser surgery or lithotripsy.

Small-amplitude structural dynamics of amorphous solids are generally described by motions on a potential energy landscape.[34] The energy landscape is a multidimensional map showing the value of the potential energy Φ at every location in the configuration space of the N-particle system. Figure 10 shows a highly simplified diagram of this landscape. An ensemble of amorphous solids inhabits an enormous number of nearly isoenergetic minima (conformational substates). The structure evolves dynamically in time as the system tunnels through or hops over barriers separating these minima.

Let us start by considering the effects of an adiabatic compression or expansion (Figure 10a and 10b), which occur so slowly that the amorphous solid remains in equilibrium at every new volume. Upon compression, the landscape's total potential energy is increased by an amount equal to the work done on the system.[35,36] The system's temperature also increases. The additional potential energy is distributed among atom pairs in an enormously complicated way which changes the entire topography, creating a new "compressed landscape",[35,36] whose local minima represent quite different structures.[35] Slow compression or expansion is a gradual evolution from one landscape to another.

Instantaneous shock compression (a limiting case) instantaneously increases the kinetic energy and pushes nonbonded atom pairs closer together.[36] There is no time for the system to surmount the barriers between conformational substates, so conformational coordinates are
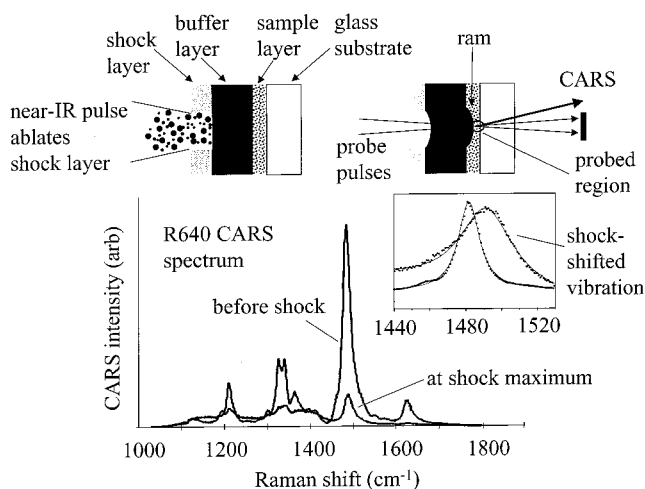
FIGURE 11. (Top) Schematic of nanoshock-driven ram impacting a thin layer of dye-doped amorphous solid on glass. (Bottom) Resonance-enhanced CARS spectrum of dye (rhodamine 640; R640) vibrational transitions with and without shock. The inset shows the vibrational frequency shift.
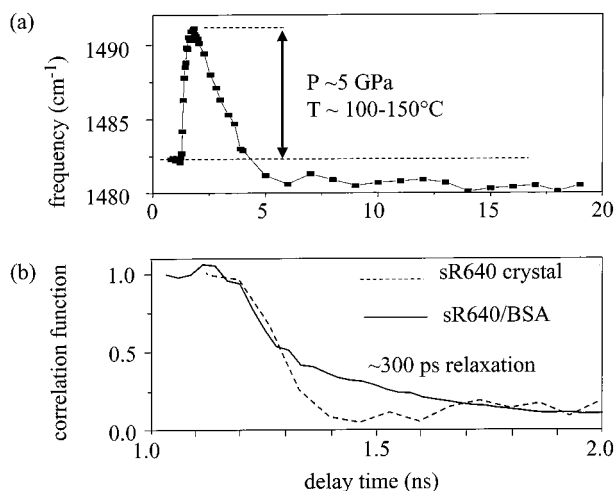

FIGURE 12. (a) Frequency shift of dye vibrational transitions in a thin layer of organic polymer, PMMA, with a ~5-GPa nanoshock. After the nanoshock, the vibrational frequency is frozen ~2 cm^{-1} to the red of its original value. (b) Intensity correlation function (eq 1) for shocked sulfarhodamine 640 dye crystals (sR640) falls at a rate determined by the shock transit time across the layer. Vibrational correlation function for sR640 in a thin dried layer of bovine serum albumin (BSA) protein shows a slower (~300 ps) component attributed to structural relaxation on the compressed energy landscape.

initially unchanged by fast shock compression.[36] Shock compression may be viewed as a vertical transition from the ambient landscape to a shocked landscape, as in Figure 10c. This vertical transition is reminiscent of, and analogous to, the Born−Oppenheimer principle for electronic transitions. The relative separations and kinetic energies of atom pairs can be changed by impact much faster than the molecular conformations. A very fast expansion (Figure 10d) may be viewed as a vertical transition downward from a shocked landscape to an ambient landscape. However, truly instantaneous expansion transitions are not possible,[4] so a real downward transition falls between the limits described in Figure 10b and 10d.

The shock energy landscape model can be used to understand the cycle of compression−heating and expansion−cooling produced by nanoshocks. When a system is shock compressed (Figure 10c), the compressed system undergoes structural relaxation on the shocked landscape (Figure 10c). This relaxation is analogous to the Stokes's shift of fluorescent molecules. A subsequent fast expansion would produce systems in the higher energy regions of the ambient landscape, as indicated in Figure 10d. Materials temporarily stuck in the higher energy regions of the ambient landscape (densified materials) can be produced by fast shock compression, leading to structural relaxation on the shocked landscape, if followed by a fast relaxation back to the ambient landscape.

Shock Experiments on Polymers and Proteins

The high sensitivity of resonance-enhanced CARS[27] of a dye probe is used so that very thin (~200 nm) sample layers can be studied to increase the time resolution. Rhodamine 640 (R640) is doped in organic polymers, and water-soluble sulfarhodamine 640 (sR640) is doped in biomolecules. A schematic of the experiment[36] is shown in Figure 11. A nanoshock drives a tiny ram (100 μm in diameter) from a polymer buffer layer into an ~200-nm-

thick sample layer on a glass substrate. Due to shock reflection from the glass, the sample sees a two-stage ~5-GPa shock,[22] whose rise time is the ~100-ps shock time for a round trip through 400 nm of material. The resonance CARS spectrum of R640 dye[37] in polymethyl methacrylate (PMMA) is shown in Figure 11. When the sample is shocked, the dye vibrational frequencies shift as shown in the inset, and the resonance CARS intensity drops significantly, because dye electronic transitions are pressure-tuned away from resonance.

The intensity decrease and vibrational shift are used as probes of local dynamics, in analogy to the way time-dependent dye spectra are used to probe solvation dynamics in liquids and glasses.[21,38] A normalized correlation function $C(t)$ is defined,[21]

$$C(t) = \frac{\Delta\alpha(t) - \Delta\alpha(pk)}{\Delta\alpha(0) - \Delta\alpha(pk)} \qquad (1)$$

where $\Delta\alpha$ is either the vibrational frequency shift or the change in CARS intensity, and $\Delta\alpha(pk)$ is the frequency shift or intensity change at the peak of shock compression.

The time dependence of the R640 vibrational frequency shift in PMMA (MW > 10^6) is shown in Figure 12a. Following the nanoshock, the vibrational frequency is frozen on the time scale of observation (~20 ns), at a value ~2 cm^{-1} to the red of its original position.

The intensity correlation function for fast compression of a thin layer of sR640 dye crystals[36] is shown in Figure 12b. The dye crystal response is essentially instantaneous, as in the anthracene experiments discussed above. The correlation function decays with the ~100-ps shock round trip time through the dye crystals.

The solid curve in Figure 12b is the vibrational shift correlation function for sR640 in a thin film of bovine serum albumin (BSA).[36] BSA is the most common protein in blood. This dried film is a crude model for biological tissues such as skin. A new feature never seen in crystals is observed in BSA and organic polymers.[36] After the rapid drop in $C(t)$ due to the front crossing the BSA, there is a subsequent decay which is approximately described by an ~150-ps time constant. This ~150-ps process is attributed to structural relaxation on the shocked energy landscape, as in Figure 10c. Owing to the short duration of the nanoshock pulse, this structural relaxation cannot be observed for much longer than ~1 ns, so we cannot say whether the decay is nonexponential in time.

The residual frequency shift after nanoshock seen in Figure 12a suggests we have produced a mechanically excited state high up the ambient potential energy landscape, as in Figure 10d. In future work, we intend to extend these measurements to longer time regimes to study structural relaxation on the ambient landscape, which is slower than relaxation on the shocked landscape because the temperature is lower and the viscosity is higher. The degree of mechanical distortion might be further increased by lengthening the nanoshock pulse and decreasing the fall time. That might be accomplished with new shock layer designs and, possibly, shaped optical pulses.

Concluding Remarks

In contrast to time-resolved optical studies of electronic state dynamics, ultrafast nanoshock spectroscopy permits a new focus on mechanical and thermal excitations. Shock wave spectroscopy is concerned with systems perturbed by large-amplitude mechanical transients, high temperatures, and high pressures. Initial applications of nanoshock spectroscopy in physical chemistry involved high explosives. However, as the organic polymer and protein work illustrates, nanoshock spectroscopy can be a powerful tool for the study of all condensed matter systems.

References

(1) Dlott, D. D.; Hambir, S.; Franken, J. The new wave in shock waves. *J. Phys. Chem. B* **1998**, *102*, 2121–2130.
(2) Graham, R. A. *Solids Under High-Pressure Shock Compression. Mechanics, Physics and Chemistry*; Springer-Verlag: New York, 1993.
(3) Dlott, D. D. Ultrafast spectroscopy of shock waves in molecular materials. *Annu. Rev. Phys. Chem.* **1999**, *50*, 251–78.
(4) Zel'dovich, Y. B.; Raiser, Y. P. *Physics of Shock Waves and High-temperature Hydrodynamic Phenomena*; Academic Press: New York, 1966.
(5) Marsh, S. P. *LASL Shock Hugoniot Data*; University of California, Berkeley: Berkeley, CA, 1980.
(6) Franken, J.; Hambir, S.; Hare, D. E.; Dlott, D. D. Shock waves in molecular solids: ultrafast vibrational spectroscopy of the first nanosecond. *Shock Waves* **1997**, *7*, 135–145.
(7) Warnes, R. H. Shock wave compression of three polynuclear aromatic compounds. *J. Chem. Phys.* **1970**, *53*, 1088–1094.
(8) Dlott, D. D.; Fayer, M. D. Shocked molecular solids: vibrational up pumping, defect hot spot formation, and the onset of chemistry. *J. Chem. Phys.* **1990**, *92*, 3798–3812.
(9) Tokmakoff, A.; Fayer, M. D.; Dlott, D. D. Chemical reaction initiation and hot-spot formation in shocked energetic molecular materials. *J. Phys. Chem.* **1993**, *97*, 1901–1913.
(10) Jindal, V. K.; Dlott, D. D. Orientation dependence of shock-induced heating in anharmonic molecular crystals. *J. Appl. Phys.* **1998**, *83*, 5203–5211.
(11) Bardo, R. D. The lattice density of states concept and its role in determining the shock sensitivity of PETN and nitromethane. In *Proceedings of the Ninth Symposium on Detonation*; Short, J. M., Ed.; 1989; Vol. I; pp 235–245.
(12) Coffey, C. S.; Toton, E. T. A microscopic theory of compressive wave-induced reactions in solid explosives. *J. Chem. Phys.* **1982**, *76*, 949–954.
(13) Tarver, C. M. Multiple roles of highly vibrationally excited molecules in the reaction zones of detonation waves. *J. Phys. Chem. A* **1997**, *101*, 4845–4851.
(14) Holian, B. L.; Straub, G. K. Molecular dynamics of shock waves in three-dimensional solids: Transition from nonsteady to steady waves in perfect crystals and implications for the Rankine-Hugoniot conditions. *Phys. Rev. Lett.* **1979**, *43*, 1598–1600.
(15) Holian, B. L.; Hoover, W. G.; Moran, B.; Straub, G. K. Shock-wave structure via nonequilibrium molecular dynamics and Navier–Stokes continuum mechanics. *Phys. Rev. A* **1980**, *22*, 2798–2808.
(16) Brenner, D. W.; Robertson, D. W.; Elert, M. L.; White, C. T. Detonation at nanometer resolution. *Phys. Rev. Lett.* **1993**, *70*, 2174–2177.
(17) Robertson, D. H.; Brenner, D. W.; White, C. T. Microscopic simulations of complex hydrodynamic phenomena. In *High-Pressure Shock Compression of Solids III*; Davison, L., Shahnipoor, M., Eds.; Springer-Verlag: New York, 1997.
(18) Tas, G.; Franken, J.; Hambir, S. A.; Dlott, D. D. Ultrafast Raman spectroscopy of shock fronts in molecular solids. *Phys. Rev. Lett.* **1997**, *78*, 4585–4588.
(19) Ng, A.; Forsman, A.; Celliers, P. Heat-front propagation in femtosecond-laser-heated solids. *Phys. Rev. E* **1995**, *51*, R5208–R5211.
(20) Swegle, J. W.; Grady, D. E. Shock viscosity and the prediction of shock wave rise times. *J. Appl. Phys.* **1985**, *58*, 692–701.
(21) Stratt, R. M.; Maroncelli, M. Nonreactive dynamics in solution: the emerging molecular view of solvation dynamics and vibrational relaxation. *J. Phys. Chem.* **1996**, *100*, 12981–12996.
(22) Hambir, S. A.; Franken, J.; Hare, D. E.; Chronister, E. L.; Baer, B. J.; Dlott, D. D. Ultrahigh time resolution vibrational spectroscopy of shocked molecular solids. *J. Appl. Phys.* **1997**, *81*, 2157–2166.
(23) Tas, G.; Hambir, S. A.; Franken, J.; Hare, D. E.; Dlott, D. D. Coherent Raman spectroscopy of nanoshocks. *J. Appl. Phys.* **1997**, *82*, 1080–1087.
(24) Cottet, F.; Romain, J. P. Formation and decay of laser-generated shock waves. *Phys. Rev. A* **1982**, *25*, 576–579.
(25) Schoen, P. E.; Campillo, A. J. Characteristics of compressional shocks resulting from picosecond heating of confined foils. *Appl. Phys. Lett.* **1984**, *45*, 1049–1051.
(26) Lee, I.-Y. S.; Hill, J. R.; Dlott, D. D. Ultrafast microscopy of shock waves using a shock target array with an optical nanogauge. *J. Appl. Phys.* **1994**, *75*, 4975–4983.
(27) Eesley, G. L. *Coherent Raman Spectroscopy*; Pergamon: Oxford, 1991.
(28) Lee, K.-Y.; Chapman, L. B.; Coburn, M. D. 3-Nitro-1,2,4-triazol-5-one, a less sensitive explosive. *J. Energ. Mater.* **1987**, *5*, 27–33.
(29) Franken, J.; Hambir, S. A.; Dlott, D. D. Ultrafast shock-induced orientation of polycrystalline films: applications to high explosives. *J. Appl. Phys.* **1999**, *85*, 2068–2074.
(30) Dick, J. J.; Mulford, R. N.; Spencer, W. J.; Pettit, D. R.; Garcia, E.; Shaw, D. C. Shock response of Pentaerythritol tetranitrate single crystals. *J. Appl. Phys.* **1991**, *70*, 3572–3587.
(31) Andersen, W. H. Approximate method of calculating critical shock initiation conditions and run distance to detonation. *Propellants, Explos., Pyrotech.* **1984**, *9*, 39–44.
(32) Bowden, F. P.; Williams, H. T. Initiation and propagation of explosion in azides and fulminates. *Proc. R. Soc. A* **1951**, *208*, 176–188.
(33) Hambir, S. A.; Kim, H.; Dlott, D. D. Ultrafast dynamics of nanoshocks in molecular materials. In *Shock Compression of Condensed Matter—1999*; Furnish, M. D., Ed.; American Institute of Physics: New York, 1999 (in press).

(34) Stillinger, F. H. A topographic view of supercooled liquids and glass formation. *Science* **1995**, *267*, 1935−1939.

(35) Malandro, D. L.; Lacks, D. J. Volume dependence of potential energy landscapes in glasses. *J. Chem. Phys.* **1997**, *107*, 5804−5810.

(36) Kim, H.; Hambir, S. A.; Dlott, D. D. Ultrafast dynamics of shock waves in polymers and proteins: the energy landscape. *Phys. Rev. Lett.*, in press.

(37) Takayanagi, M.; Hamaguchi, H.; Tasumi, M. Probe-frequency dependence of the resonant inverse Raman band shape. *J. Chem. Phys.* **1988**, *89*, 3945−3950.

(38) Berg, M. A viscoelastic continuum model of nonpolar solvation. I. Implications for multiple time scales in liquid dynamics. *J. Phys. Chem. A* **1998**, *102*, 17−30.

AR970260U